IOPscience iopscience.iop.org

Home Search Collections Journals About Contact us My IOPscience

Evidence for the formation of GaAs homojunction far-infrared detection by magnetic field dependent Hall analysis

This article has been downloaded from IOPscience. Please scroll down to see the full text article.

2004 J. Phys.: Condens. Matter 16 997

(http://iopscience.iop.org/0953-8984/16/6/027)

View the table of contents for this issue, or go to the journal homepage for more

Download details:
IP Address: 129.252.86.83
The article was downloaded on 27/05/2010 at 12:42

Please note that terms and conditions apply.

INSTITUTE OF PHYSICS PUBLISHING JOURNAL OF PHYSICS: CONDENSED MATTER

J. Phys.: Condens. Matter **16** (2004) 997–1006 PII: S0953-8984(04)71045-0

Evidence for the formation of GaAs homojunction far-infrared detection by magnetic field dependent Hall analysis

X Y Chen and W Z Shen[1]

Laboratory of Condensed Matter Spectroscopy and Opto-Electronic Physics, Department of Physics, Shanghai Jiao Tong University, 1954 Hua Shan Road, Shanghai 200030, People's Republic of China

E-mail: wzshen@sjtu.edu.cn

Received 24 October 2003
Published 30 January 2004
Online at stacks.iop.org/JPhysCM/16/997 (DOI: 10.1088/0953-8984/16/6/027)

Abstract
Experimental magnetic field dependent Hall and resistivity data are presented for n-GaAs homojunction far-infrared (FIR) detector structures in the temperature range from 1.8 to 200.0 K and with a magnetic field up to 15 T. The carrier transport properties of the multilayer/multicarrier structure have been separated and quantified individually by a hybrid approach consisting of mobility spectrum analysis followed by a multicarrier fitting procedure. The observed temperature dependence of mobility and concentration is explained using classical band theory, which unambiguously reveals highly doped degenerate contact layers and semiconductor–metal transition in emitter layers. The detailed analysis of the concentration and the Fermi level in the emitter layers gives clear evidence for the formation of GaAs homojunction FIR detection occurring at the interfaces between the emitter and intrinsic layers.

1. Introduction

High performance far-infrared (FIR) semiconductor detectors and arrays with a cutoff wavelength λ_c ranging from a few tens to a few hundreds of micrometres are critically required for FIR spectroscopy and FIR remote sensing in space [1]. In recent years, homojunction FIR detectors based on the mature materials GaAs [2] and Si [3] have been demonstrated, and they have received much interest. The detector operation is based on internal photoemission occurring at the interface between the main detection structure of a doped absorber (emitter) layer and an undoped intrinsic layer across which most of the external bias is dropped. The λ_c is determined by the interfacial barrier height, which depends on the doping concentration of emitter layers and applied biases. The homojunction FIR detectors may have a performance

[1] Author to whom any correspondence should be addressed.

 © 2004 IOP Publishing Ltd Printed in the UK

comparable to that of conventional Ge (unstressed or stressed) photoconductors [2, 4, 5], with a unique material advantage. Recent progress has been made on n-GaAs homojunction FIR detector structures by

(i) the observation that n-GaAs is more suitable for a long λ_c detector design due to a considerably low doping level in the emitter layers [6],
(ii) the measurement of a true optical field distribution within the FIR detector structures [7], and
(iii) the suggestion, optimization and demonstration of bottom mirrors for resonant cavity enhanced (RCE) n-GaAs FIR detectors to increase the photon absorption [8].

The analysis of carrier transport properties has proved to be a powerful tool for the investigation of semiconductors [9]. An accurate determination of the electrical parameters is very useful for the better understanding and further improvement of device performance [10]. However, little information about the electronic transport parameters (mobility and concentration) is available for homojunction FIR detector structures. In particular, there is no direct experimental evidence for the formation of the homojunction FIR detection at the emitter/intrinsic interfaces. The homojunction FIR detectors are based on multilayer structures with different doping levels. It is clear that layers with different doping concentrations will have different concentration and mobility characteristics. The contribution of the emitter layers to the total electronic transport must be separated from that of the contact layers, in order to have a clear and complete understanding of the carrier transport process within the interfaces between the emitter and intrinsic layers.

In this paper, we report on the experimental results and theoretical analysis of magnetic field dependent Hall and resistivity data for RCE n-GaAs homojunction FIR detector structures. A hybrid approach, which consists of mobility spectrum analysis (MSA) followed by a multicarrier fitting (MCF) procedure [11–13], has been employed to extract the individual carrier transport parameters present in the multilayer/multicarrier structure with different doping concentrations. In addition to the well explained temperature-dependent mobility and concentration characteristics by classical band theory, clear evidence has been provided for the formation of GaAs homojunction FIR detection occurring at the emitter/intrinsic interfaces.

2. Experiments

The RCE GaAs homojunction FIR detector sample (n doped by silicon) was grown by molecular beam epitaxy (MBE) on a semi-insulating (SI) GaAs substrate (SUB). Figure 1 shows a schematic view of the multilayer structure. The main detection (MD) structure, which consists of several periods of doped emitter layers (1×10^{17} cm^{-3}) and undoped intrinsic layers for the internal photoemission, is sandwiched between the top mirror (TM) and the recently proposed undoped/doped GaAs bottom mirror (BM) structures [8]. Ohmic contacts can be easily formed in highly doped (2–3×10^{18} cm^{-3}) layers of the top and bottom mirrors, which also serve as the top and bottom contact layers for the FIR detector. It is clear that the multilayer detector structure contains two populations of distinct carrier (electron) species. Another sample with only the BM structure (i.e., without the MD and TM structures) has also been grown and measured for comparison. This BM-only structure has only one electron species (2–3×10^{18} cm^{-3}).

The dark Hall measurements were performed in a Van der Pauw configuration by a set of Keithley Hall measurement system, including a 220 programmable current source, 2182 nanovoltmeter and 7001 switch system with a 7065 Hall card. The ohmic contacts were fabricated by alloying indium on the surfaces of the two GaAs multilayer structures. The Hall

Layer	Structure	
TM	n^{++} 2×10^{18} cm^{-3} GaAs 100nm	
MD	n^{+} 1×10^{17} cm^{-3} GaAs 200nm	
	i GaAs 100nm	×10
	n^{+} 1×10^{17} cm^{-3} GaAs 30 nm	
	i GaAs 150nm	
	n^{+} 1×10^{17} cm^{-3} GaAs 200nm	
BM	n^{++} 2×10^{18} cm^{-3} GaAs 300nm	
	i GaAs 1450nm	
	n^{++} 3×10^{18} cm^{-3} GaAs 1800nm	
SUB	GaAs SI Sub.	

Figure 1. Schematic view of the resonant cavity enhanced n-GaAs multilayer FIR detector structure grown by MBE. TM: the top mirror; MD: the main detection structure; BM: the bottom mirror; and SUB: the GaAs semi-insulating substrate.

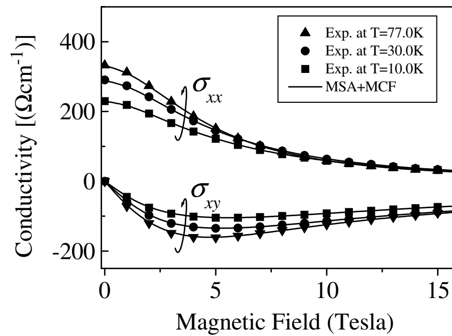

Figure 2. The experimental conductivity tensor components $\sigma_{xx}(B)$ and $\sigma_{xy}(B)$ as a function of magnetic field B at different temperatures. The solid curves are the calculated results by using the final mobility spectra derived from a hybrid approach combining MSA with an MCF procedure.

coefficient and resistivity were measured in a temperature range from 1.8 to 200.0 K under an Oxford Instruments superconductive magnet with a magnetic field up to 15 T. The field reading accuracy was better than 1%.

3. Results and discussion

Figure 2 presents the magnetic field (B) dependence of the experimental results (scattering points), in the form of conductivity component $\sigma_{xx}(B)$ and $\sigma_{xy}(B)$, under different temperatures for the RCE n-GaAs multilayer detector structure. The solid curves are the calculated $\sigma_{xx}(B)$ and $\sigma_{xy}(B)$ obtained using the carrier concentrations and mobility distributions to be discussed in detail below. The experimental fact that we have observed negative values of $\sigma_{xy}(B)$ throughout the magnetic field reflects the n-type nature of the measured sample, which is in agreement with the MBE design of the multilayer structure. It should be noted that the traditional method of fixed magnetic field Hall measurements

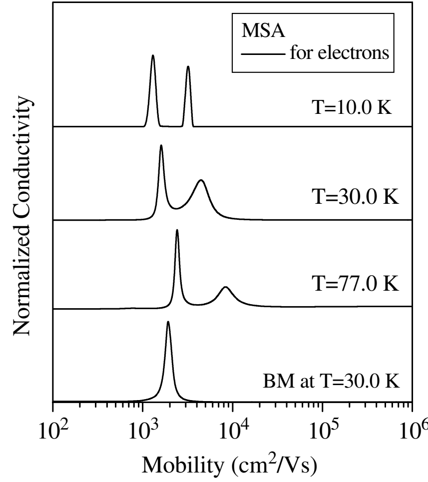

Figure 3. Temperature-dependent mobility spectra obtained by using MSA for the n-GaAs multilayer FIR detector structure, together with a mobility spectrum of the BM-only sample at 30.0 K for comparison.

cannot be employed for the multilayer structure with different doping concentrations, since the yielded carrier information only represents the average carrier concentration and mobility of the sample, and the measured Hall coefficient and resistivity are not constant with respect to the magnetic filed [11]. In our multilayer structure, layers with different doping concentrations will show different concentration and mobility characteristics. Consequently, it is necessary to employ variable magnetic field Hall measurements and multicarrier analysis, in order to extract the true carrier information in the multilayer detector structure. As a result, the transport information in the emitter layers can be quantified individually, which paves the way for better understanding of the FIR detection mechanisms.

In order to extract the transport parameters of all carrier species present within the sample that are contributing to the conduction process, we employ a hybrid approach combining MSA with MCF [11–13] procedures. In the MSA approach, discrete carriers are generalized by a conductivity concentration function that spreads over a continuous mobility (μ) range. The two conductivity tensors are given by

$$\begin{aligned}\sigma_{xx}(B) &= \frac{\rho(B)}{\rho^2(B)+B^2R_{\mathrm{H}}^2(B)} = \int_0^\infty \frac{s^{\mathrm{p}}(\mu)+s^{\mathrm{n}}(\mu)}{1+\mu^2B^2}\,\mathrm{d}\mu \\ \sigma_{xy}(B) &= \frac{BR_{\mathrm{H}}(B)}{\rho^2(B)+B^2R_{\mathrm{H}}^2(B)} = \int_0^\infty \frac{(s^{\mathrm{p}}(\mu)-s^{\mathrm{n}}(\mu))\mu B}{1+\mu^2B^2}\,\mathrm{d}\mu\end{aligned} \quad (1)$$

where $R_{\mathrm{H}}(B)$ and $\rho(B)$ are the experimental magnetic field dependent Hall coefficient and resistivity, respectively, and $s^{\mathrm{p}}(\mu)$ and $s^{\mathrm{n}}(\mu)$ are hole and electron conductivity concentration functions, respectively. The MSA would transform the above experimental magnetic field dependent Hall data into the dependence of the conductivity concentration function on the mobility, in which each kind of carrier contributing to the total conductivity appears as a separate peak at a given mobility [11–13]. By MSA, we can obtain the number of carrier species as well as the corresponding rough mobility and concentration.

Figure 3 shows the corresponding normalized mobility spectrum obtained via the MSA procedure from the experimental $\sigma_{xx}(B)$ and $\sigma_{xy}(B)$ in figure 2, together with a mobility spectrum for the BM-only sample at 30 K for comparison. For the BM-only sample, there is

only one peak in the mobility spectrum by MSA, revealing only one electron species there. This is reasonable, since there is only one highly doping concentration ($2–3 \times 10^{18}$ cm^{-3}) in the multilayer structure. The peak corresponds to an effective average value of the two highly doped layers, which dominate the conductivity. The contributions of the undoped GaAs layer and the GaAs SI substrate to the conductivity can be ignored. The mobility value of 1.9×10^3 cm^2 V^{-1}s^{-1} is in good agreement with the previously reported result of $\sim 2.0 \times 10^3$ cm^2 V^{-1} s^{-1} for the same doping level of n-GaAs in [14]. In contrast, we can clearly observe two electron peaks in the mobility spectra of the multilayer detector sample throughout the measured temperature; i.e., two electron species can be identified in the studied detector sample. By taking into account the doping levels in the detector structure and the comparison measurements, we can easily assign the low mobility carrier to the highly doped ($2–3 \times 10^{18}$ cm^{-3}) contact layers in the TM and BM structures, and attribute the high mobility carrier to the emitter (1×10^{17} cm^{-3}) layers in the MD structure.

At a temperature of 77 K, the conductivity of the emitter layers is much less than that associated with the highly doped contact layers. As the temperature is decreased, the conductivity of the emitter layers increases relative to that of the contact layers. The dramatically different temperature dependence of the conductivity in the emitter layers is directly associated with the semiconductor–metal transition in the emitter layers for the formation of internal photoemission occurring at the interfaces between the emitter and intrinsic layers in the homojunction FIR detectors [15] (we will discuss this in detail below). Furthermore, MSA reveals a minor hole peak at $T = 1.8$ K, in addition to the above-mentioned two electron species. However, the minor hole peak is an artefact result, since MSA may not provide an adequate description of the conductivity at extremely low temperature and high magnetic field, where both $s(\mu)$ and $\sigma(B)$ oscillate with B (Shubnikov–de Haas oscillations) [11]. On the other hand, with the decrease of temperature, the extracted mobility values in these two electron species both decrease as a result of the increased ionized impurity scattering at temperatures below 100 K.

It should be noted that the accurate carrier concentration and mobility of every carrier species cannot be completely determined only by the MSA procedure, because of the limitation of the finite magnetic field in the Hall experiments [11, 12]. Accurate carrier information can be obtained by the MCF procedure for the two conductivity tensor components $\sigma_{xx}(B)$ and $\sigma_{xy}(B)$ with the given carrier species number (m-carrier system), and the initial carrier concentration and mobility values from the MSA. The expression for MCF is

$$\sigma_{xx}(B) = \sum_{i=1}^{m} \frac{en_i\mu_i}{1+\mu_i^2B^2}, \qquad \sigma_{xy}(B) = \sum_{i=1}^{m} S_i \frac{en_i\mu_i^2B}{1+\mu_i^2B^2} \tag{2}$$

where n_i and μ_i are the concentration and mobility of the ith carrier species, respectively, e is the electron charge, and S_i is the sign of the charge (+1 for holes and -1 for electrons). The solid curves in figure 2 are the two-electron fitting results, which are clearly in good agreement with the experimental data. Figures 4 and 5 show the exact temperature-dependent carrier mobility and concentration of the two electron species in the detector sample, respectively. In those two figures, the experimental carrier information from the highly doped contact layers and the emitter layers has been denoted by filled squares and circles, respectively.

For the temperature-dependent mobility, it is commonly accepted that two most important mechanisms in semiconductors that limit mobility are ionized impurity scattering below 100 K and phonon scattering above 100 K. Recently, another temperature-independent scattering mechanism has been proposed [16] and superposed on the ionized impurity and phonon scattering mechanisms. The resulting total mobility (μ_{total}) in semiconductors is then given

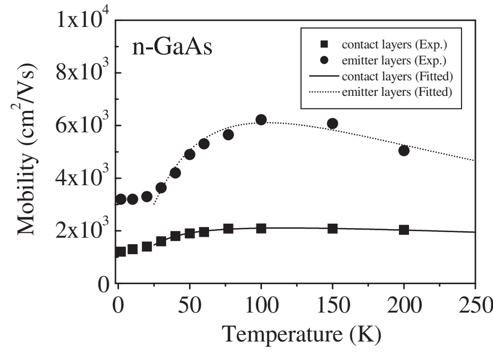

Figure 4. The temperature dependence of electron mobility for the highly doped contact layers (experimental results: filled squares; fitting results: the solid curve) and the emitter layers (experimental results: filled circles; fitting results: the dotted curve).

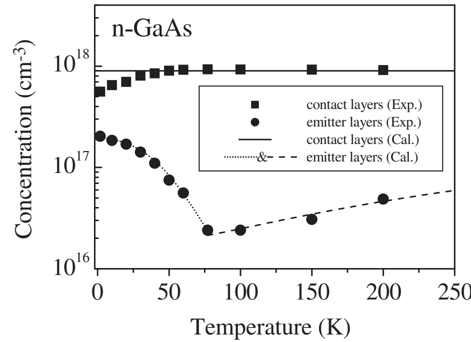

Figure 5. The temperature dependence of electron concentration for the highly doped contact layers (experimental results: filled squares; fitting results: the solid curve) and the emitter layers (experimental results: filled circles; fitting results: the dotted and dashed curves).

by

$$\mu_{\rm total}^{-1} = \mu_{\rm imp}^{-1} + \mu_{\rm pho}^{-1} + \mu_{\rm TI}^{-1} \tag{3}$$

where $\mu_{\rm imp}$ and $\mu_{\rm pho}$ are the contribution from the ionized impurity scattering and phonon scattering with the temperature dependence of $AT^{3/2}$ and $BT^{-3/2}$, respectively, and $\mu_{\rm TI}$ is the temperature-independent term with the possible contributing mechanisms of structural features [16], such as surface roughness, dislocation strain fields, and neutralized impurities. In our experiments, the electron mobility in the highly doped layers is approximately a constant of 2.0×10^3 cm^2 V^{-1} s^{-1} for temperatures above 30 K, and decreases slightly with temperature below 30 K. In contrast, the emitter layers demonstrate a broader mobility peak (with a peak value of 6.2×10^3 cm^2 V^{-1} s^{-1} at 100 K), revealing the characteristics with lattice scattering dominating at temperatures $T > 100$ K and scattering on ionized impurities being dominant for $T < 100$ K. Furthermore, these temperature-dependent values are in good agreement with the separately reported mobility in n-GaAs films with doping levels of $\sim 10^{17}$–10^{18} cm^{-3} [17, 18]. These results reveal the three-dimensional (3D) characteristics of the carriers.

The solid and dotted curves in figure 4 are the fitting results from equation (3), which can well explain the observed temperature-dependent experimental mobility in the temperature range 30–200 K. The fitting parameters are: $A = 30.5$ cm^2 V^{-1} s^{-1} K$^{-3/2}$,

$B = 4.8 \times 10^7$ $K^{3/2}$ cm^2 V^{-1} s^{-1}, $\mu_{TI} = 2400$ cm^2 V^{-1} s^{-1} for the highly doped contact layers, and $A = 37.0$ cm^2 V^{-1} s^{-1} $K^{-3/2}$, $B = 4.2 \times 10^7$ $K^{3/2}$ cm^2 V^{-1} s^{-1}, $\mu_{TI} = 8900$ cm^2 V^{-1} s^{-1} for the emitter layers. It is the large difference in μ_{TI} that results in the different temperature dependence of the mobility between the contact and emitter layers. In our MBE grown multilayer structure, the main mechanism of the temperature-independent term is the neutralized impurity scattering. It is well known that there are unionized impurities in the doped layers, and the amount is strongly related with the doping level. We have also observed that the ionized process is weak or even absent in such doping levels (above 10^{17} cm^{-3}) of n-GaAs (see figure 5). As a result, the unionized impurity concentration in the highly doped contact layers is much higher than that in the emitter layers. Nevertheless, it should be noted that the above model cannot be employed in the case of low temperature below 20 K, where the observed mobility is much higher than that predicted by equation (3). This is mainly due to the fact that the screening by electrons and neighbouring impurities should be taken into account at extremely low temperatures, as already pointed out in the Brooks–Herring theory [19].

For the experimental concentration shown in figure 5, it is clear that the electron concentration in the highly doped contact layers is also almost independent of temperature. The electron concentration remains at the order of 10^{18} cm^{-3} (i.e., 9.1×10^{17} cm^{-3} at 200 K), which is very close to the designed doping level of $(2–3) \times 10^{18}$ cm^{-3} at room temperature. The BM-only sample almost shows the same behaviour as that of the contact layers. This behaviour is characteristic of a nonthermally activated conduction process, implying that for such heavily doped n^{++}-GaAs layers the material is either degenerate or carrier transport is proceeding via an impurity band. However, the observed almost constant mobility with increasing temperature (from 30 to 200 K in figure 4) clearly excludes the possibility of impurity band conduction, where the experimental mobility value should increase slightly with temperature [20]. For the degenerate case, we can employ the following general expression for the electron concentration (n) to estimate the Fermi level E_F in the highly doped contact layers:

$$n = 2\left(\frac{2\pi m^* k_B T}{h^2}\right)^{3/2} F_{1/2}(\eta) \tag{4}$$

with m^* the effective mass of electrons, k_B Boltzmann's constant, h Planck's constant, and T the temperature. $F_{1/2}(\eta)$ is the Fermi integral with the reduced Fermi level η in the conduction band E_C: $\eta = (E_F - E_C)/k_B T$. Under the assumption that all the free electrons are located in the conduction band, we obtain the reduced Fermi level η of 2.67 at 200 K, which will become higher at lower temperatures. This further demonstrates that the electrons are strongly degenerate there. At a strongly degenerate limit, equation (4) can be simplified as

$$n = \frac{8\pi}{3}\left(\frac{2m^* E_F^n}{h^2}\right)^{3/2} \tag{5}$$

with the Fermi energy $E_F^n = E_F - E_C$. The solid line in figure 5 is the calculated electron concentration (via equation (5)) with the Fermi energy E_F^n of 51.0 meV and m^* of $0.0668m_0$. A good agreement with the experimental concentration is observed with only a small deviation at the extremely low temperature below 20 K.

Of particular interest is the experimental fact that the temperature dependence of the electron concentration in the emitter layers is dramatically different from that of the highly doped contact layers. The observed concentration varies in the range of 10^{16}–10^{17} cm^{-3}, which is also close to the doping level of 1×10^{17} cm^{-3}. At high temperatures ($T > 100$ K), the reduced Fermi level η for the emitter layers is less than -1, revealing that the Fermi level is below the conduction band. The concentration increases from 2.4×10^{16} cm^{-3} at 100 K to 4.9×10^{16} cm^{-3} at 200 K. The temperature dependence of electron concentration

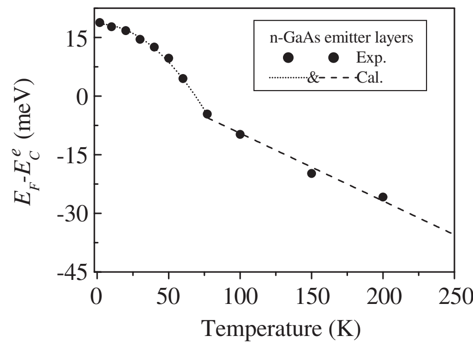

Figure 6. The calculated Fermi energy as a function of temperature in the emitter layers (experimental results: filled circles; fitting results: the dotted and dashed curves).

shows characteristics of thermally activated electrons from a donor level to the conduction band, i.e., a typically weak ionized process. In contrast, at temperature below 100 K, the electron concentration increases abnormally with the decrease of temperature, and reaches to 2.0×10^{17} cm^{-3} at 1.8 K.

By using the obtained electron concentrations in the emitter layers, we have also calculated the Fermi energy under different temperatures through equation (4), as shown in figure 6. We have found that the Fermi energy increases rapidly with the decrease of temperature, from −25.8 meV at 200 K to +18.8 meV at 1.8 K. Therefore, as the Fermi level emerges into the conduction band, a semiconductor–metal transition takes place gradually in the emitter layers with the decrease of temperature. A similar semiconductor–metal transition has also been reported in GaSb/AlGaSb multiple quantum well structures [21]. Furthermore, the temperature dependence of the Fermi energy in the emitter layers will demonstrate different behaviours due to the semiconductor–metal transition, i.e., near square dependence in the degenerate semiconductor [22] and near linear dependence in the nondegenerate semiconductor case [23]. The dotted curves in figures 5 and 6 are the calculated electron concentration and Fermi energy by using the square dependence, while the dashed curves are for linear Fermi energy. It is clear that the calculated results can well describe the temperature-dependent experimental data, which gives further support for the transition assignment and the formation of space charge accumulation.

We have deduced experimentally the band gap shrinkage of $-3.4 \pm 0.2 \times 10^{-8}$ (eV cm)$N^{1/3}$ (with N the carrier concentration) for n-GaAs [6]. At a temperature of 30 K, we have obtained the Fermi energy $E_{\mathrm{F}} - E_{\mathrm{C}}^{\mathrm{e}}$ of ∼14.5 meV in the emitter layers. The Fermi energy is smaller than the band gap shrinkage $E_{\mathrm{C}}^{\mathrm{i}} - E_{\mathrm{C}}^{\mathrm{e}}$ of ∼21.1 meV, which results in the fact that the Fermi level E_{F} is merged into the conduction band $E_{\mathrm{C}}^{\mathrm{e}}$, but is still below the conduction band edge of the intrinsic layers $E_{\mathrm{C}}^{\mathrm{i}}$. Based on the above transport results and the FIR detection mechanism, we depict in figure 7 the energy band diagrams of the emitter/intrinsic interface layers under applied biases, which clearly reveal the different Fermi energies at different temperatures.

At the emitter/intrinsic interfaces, the electron is transferred to the intrinsic layers with the positively charged fixed donors retained in the emitter layers due to the different work-functions between the emitter and intrinsic layers [24]. In the meantime, due to the band gap narrowing effect, the band gap shrinkage happens in the emitter layers, and an interfacial barrier has been formed at the emitter/intrinsic interface below 30 K (figure 7(a)). The internal photoemission operation is that electrons are photoexcited from the emitter layers into the intrinsic layers.

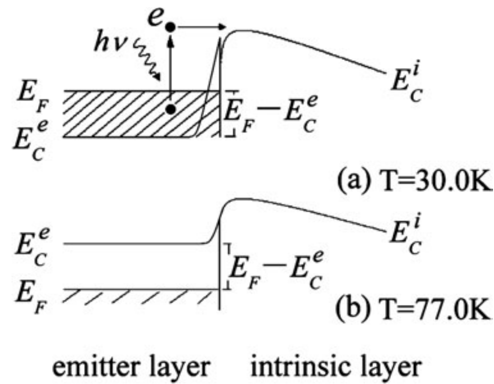

Figure 7. Energy band diagrams for the interface between the emitter layer and intrinsic layer under applied biases at two typical temperatures (without considering the image force effect), where the different Fermi levels in the emitter layer are clearly revealed at different temperatures.

We have demonstrated [25] that the cutoff wavelength of the actual FIR response of GaAs device structures can be described well by the modelled band structure for the interfacial barrier height with respect to the Fermi level (it mainly depends on the doping concentration of the emitter layers and the applied bias). With increasing temperature, the Fermi level gradually moves downwards below the conduction band of the emitter layers (figure 7(b)). Therefore, our electron transport characteristics for the emitter layers show clear experimental evidence for the previously assumed formation of the homojunction FIR detection [15] due to the temperature-induced Fermi level shift. This also explains the experimental fact that we can only detect FIR radiation below 30–40 K in the homojunction FIR detectors.

Finally, it is noted that we could not observe the similar positive space charge between the highly doped contact layer and the undoped layer in both the BM-only sample and the FIR detector structure. This is due to the fact that the n^{++} contact layers are degenerate and the Fermi level ($E_{\rm F}^n = 51.0$ meV) is well above the conduction band edge of the intrinsic layers ($E_{\rm C}^{\rm i}$). This type of device works in the mid-infrared and long wavelength infrared range [15], and has been demonstrated by Tohyama *et al* [26].

4. Conclusions

The electron transport properties of RCE n-GaAs homojunction FIR detector structures grown by MBE are investigated by variable magnetic field Hall measurements for temperatures ranging from 1.8 to 200.0 K. The individual carrier transport parameters of the highly doped contact layers and the emitter layers have been extracted from the multilayer/multicarrier structure by a hybrid approach consisting of MSA followed by an MCF procedure. Due to the high doping level, the electrons show a classical degenerate behaviour in the contact layers, in which the electron concentration and mobility are almost independent of temperature. In contrast, the observed electron concentration in the emitter layers demonstrates an interesting phenomenon, which has been assigned to be related with the semiconductor–metal transition at low temperatures. This transition, due to the temperature-induced Fermi level shift, is the base for the formation of the homojunction FIR detection. Through the discussion of the homojunction detection mechanisms and a detailed analysis of the observed transport properties, we have shown clear experimental evidence for the formation of the homojunction FIR detection in the studied multilayer structure.

Acknowledgments

This work was supported in part by the Natural Science Foundation of China under contract Nos 10125416, 60006005 and 10304010, the HYD (No. 81005) and TRAPOYT of the National Minister of Education. The authors would like to acknowledge Dr Y S Gui at the National Laboratory for Infrared Physics, Chinese Academy of Sciences, and Mr H B Ye at Shanghai Jiao Tong University for their technical help.

References

[1] Werner M W 1994 *Infrared Phys. Technol.* **35** 539
[2] Shen W Z, Perera A G U, Liu H C, Buchanan M and Schaff W J 1997 *Appl. Phys. Lett.* **71** 2677
[3] Perera A G U, Shen W Z, Liu H C, Buchanan M, Tanner M O and Wang K L 1998 *Appl. Phys. Lett.* **72** 2307
[4] Haller E E 1994 *Infrared Phys. Technol.* **35** 127
[5] Beeman J W and Haller E E 1994 *Infrared Phys. Technol.* **35** 827
[6] Luo H T, Shen W Z, Zhang Y H and Yang H F 2002 *Physica* B **324** 379
[7] Luo H T, Zhang Y H, Shen W Z, Ding Y and Yu G 2002 *Appl. Opt.* **41** 6537
[8] Zhang Y H, Luo H T and Shen W Z 2003 *Appl. Phys. Lett.* **82** 1129
[9] See e.g., Seeger K 1973 *Semiconductor Physics* (Wien: Springer)
[10] See e.g., Sze S M 1981 *Physics of Semiconductor Devices* 2nd edn (New York: Wiley)
[11] Beck W A and Anderson J R 1987 *J. Appl. Phys.* **62** 541
[12] Antoszewski J, Dell J M, Faraone L, Tan L S, Raman A, Chua S J, Holmes D S, Lindemuth J R and Meyer J R 1997 *Mater. Sci. Eng.* B **44** 65
[13] Gui Y S, Guo S L, Zheng G Z, Chu J H, Fang X H, Qiu K and Wang X W 2000 *Appl. Phys. Lett.* **76** 1309
[14] Anderson D A, Apsley N, Davies P and Giles P L 1985 *J. Appl. Phys.* **58** 3059
[15] Perera A G U, Yuan H X and Francombe M H 1995 *J. Appl. Phys.* **77** 915
[16] Gopal V, Souw V, Chen E-H, Kvam E P, McElfresh M and Woodall J M 2000 *J. Appl. Phys.* **87** 1350
[17] Jalil A, Chevallier J, Azoulay R and Mircea A 1986 *J. Appl. Phys.* **59** 3774
[18] Szmyd D M, Hanna M C and Majerfeld A 1990 *Appl. Phys. Lett.* **68** 2376
[19] Brooks H 1955 *Advances in Electronics and Electron Physics* vol 7, ed L Marton (New York: Academic) p 85
[20] Saitoh M 1970 *J. Phys. Soc. Japan* **29** 1470
[21] Ghezzi C, Cioce B, Magnanini R and Parisini A 2001 *J. Appl. Phys.* **90** 5166
[22] Pananakakis G, Ghibaudo G, Kies R and Papadas G 1995 *J. Appl. Phys.* **78** 2635
[23] Bube R H, Benatar L and Redfield D 1994 *J. Appl. Phys.* **75** 1571
[24] Kuznicki Z T 1991 *J. Appl. Phys.* **69** 6526
[25] Shen W Z, Perera A G U, Francombe M H, Liu H C, Buchanan M and Schaff W J 1998 *IEEE Trans. Electron Devices* **45** 1671
[26] Tohyama S, Teranishi N, Kounma K, Nishimura M, Asai K and Oda E 1988 *IEDM Tech. Dig.* 82